nature materials

ARTICLES

PUBLISHED ONLINE: 7 MARCH 2016 | DOI: 10.1038/NMAT4570

# Biodegradable scaffold with built-in vasculature for organ-on-a-chip engineering and direct surgical anastomosis

Boyang Zhang[1,2], Miles Montgomery[1,2], M. Dean Chamberlain[2], Shinichiro Ogawa[3], Anastasia Korolj[1,2], Aric Pahnke[1,2], Laura A. Wells[2], Stéphane Massé[4], Jihye Kim[5], Lewis Reis[2], Abdul Momen[6], Sara S. Nunes[2,6,7], Aaron R. Wheeler[2,5], Kumaraswamy Nanthakumar[4], Gordon Keller[3], Michael V. Sefton[1,2] and Milica Radisic[1,2,6,7]*

**We report the fabrication of a scaffold (hereafter referred to as AngioChip) that supports the assembly of parenchymal cells on a mechanically tunable matrix surrounding a perfusable, branched, three-dimensional microchannel network coated with endothelial cells. The design of AngioChip decouples the material choices for the engineered vessel network and for cell seeding in the parenchyma, enabling extensive remodelling while maintaining an open-vessel lumen. The incorporation of nanopores and micro-holes in the vessel walls enhances permeability, and permits intercellular crosstalk and extravasation of monocytes and endothelial cells on biomolecular stimulation. We also show that vascularized hepatic tissues and cardiac tissues engineered by using AngioChips process clinically relevant drugs delivered through the vasculature, and that millimetre-thick cardiac tissues can be engineered in a scalable manner. Moreover, we demonstrate that AngioChip cardiac tissues implanted with direct surgical anastomosis to the femoral vessels of rat hindlimbs establish immediate blood perfusion.**

Recapitulating vascular interfaces of different organs in three dimensions is critical in both organ-on-a-chip[1–3] and tissue engineering applications[4–8]. Three-dimensional (3D) microtissues composed of parenchymal cells have often been studied in the absence of vasculature[9–11], whereas vasculature-on-a-chip has primarily been studied separately from the parenchymal cells[12–14]. A similar vascularization challenge has been experienced on the macroscale. Numerous tissue types have been successfully engineered *in vitro*, but clinical translation has been achieved only for thin tissues or those with a low metabolic demand (for example, skin, cartilage and bladder)[15]. Large solid tissues (for example, myocardium and liver) are highly sensitive to oxygen levels and become vulnerable within hours without oxygen supply[15–17]. These tissues would greatly benefit from rapid vascularization *in vitro* and direct vascular integration *in vivo*. Although elegant approaches have been described that enable anastomosis of oriented engineered capillaries to the host vasculature with perfusion several days after implantation[18], direct surgical anastomosis with immediate perfusion of vascularized tissues has been demonstrated only using vascular explants[19,20], requiring multiple surgeries to harvest the vascular bed.

Vascular networks can be engineered with subtractive fabrication by embedding a sacrificial carbohydrate–glass lattice[3,21], Pluronic F127 (ref. 3), dry alginate fibres[22], or gelatin[23] in hydrogels. However, the soft hydrogel provides only temporary structural support for the fragile hollow network and does not permit extensive tissue remodelling[21], which inevitably alters the hydrogel structure and collapses the embedded network. Synthetic biodegradable polymers could provide sufficient structural support to the engineered vessels, but their low permeability prevents biomolecule exchange and cell migration between the vessels and the parenchymal space[24–26].

To accommodate these two opposing material criteria, we created AngioChip, a stable biodegradable scaffold with a built-in branching microchannel network featuring two unique advances realized by our new 3D stamping technique. First, the synthetic built-in vascular walls were thin and flexible, yet strong enough to mechanically support a perfusable vasculature in a contracting tissue and enable direct surgical anastomosis. Second, to allow efficient molecular exchange and cell migration, nanopores and micro-holes were incorporated into the vascular walls. By establishing a stable, permeable, vessel network within AngioChips, we were liberated from material constraints, enabling the use of various extracellular matrices (ECMs) with cells in the parenchymal space and tissue remodelling. The AngioChip parenchymal space structure was also fine-tuned to mimic the anisotropy of native tissues (for example, myocardium), traditionally difficult to achieve with a homogeneous hydrogel. On the basis of this methodology, we created functional and vascularized cardiac and hepatic tissues.

## AngioChip scaffold with branching interconnected lumen

The AngioChip scaffolds were constructed using a biodegradable elastomer, poly(octamethylene maleate (anhydride) citrate) (POMaC; Fig. 1)[27,28]. POMaC was selected because it is ultraviolet-polymerizable, allowing rapid assembly under mild conditions;

[1]Department of Chemical Engineering and Applied Chemistry, University of Toronto, Toronto, Ontario M5S 3E5, Canada. [2]Institute of Biomaterials and Biomedical Engineering, University of Toronto, Toronto, Ontario M5S 3G9, Canada. [3]McEwen Center for Regenerative Medicine, Toronto, Ontario M5G 1L7, Canada. [4]The Toby Hull Cardiac Fibrillation Management Laboratory, Toronto General Hospital, Toronto, Ontario M5G 2C4, Canada. [5]Department of Chemistry, University of Toronto, Toronto, Ontario M5S 3H6, Canada. [6]Toronto General Research Institute, University Health Network, Toronto, Ontario M5G 1L7, Canada. [7]The Heart and Stroke/Richard Lewar Centre of Excellence, Toronto, Ontario M5G 1L7, Canada. *e-mail: m.radisic@utoronto.ca

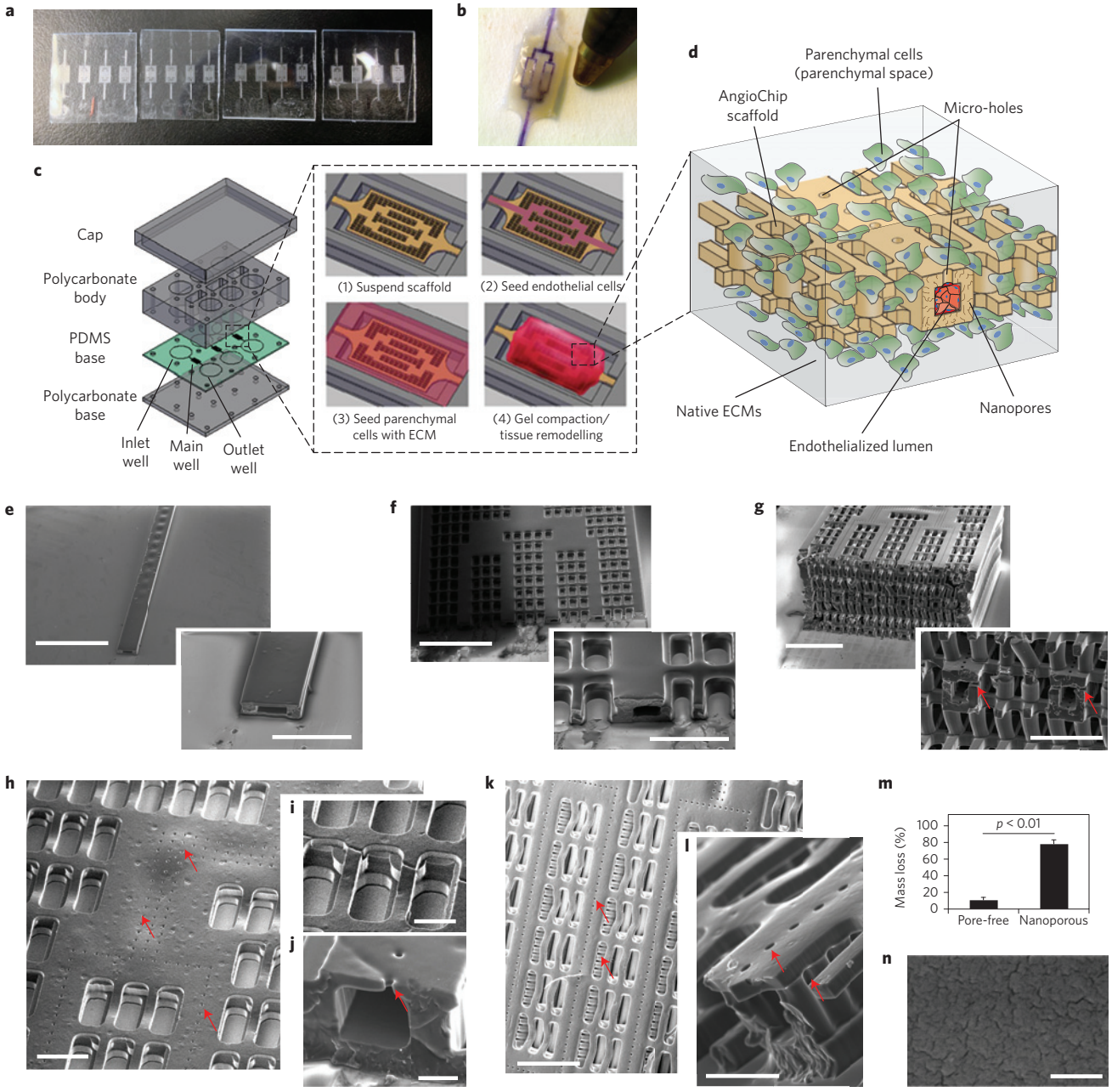


**Figure 1 | AngioChip scaffold fabrication and visualization. a**, Image of multiple AngioChip scaffolds patterned in parallel on glass slides. **b**, Image of an AngioChip hepatic tissue, perfused with a colour dye, beside the tip of a ballpoint pen for scale. **c**, Schematic of the assembly of the bioreactor and the assembly of vascularized tissue. **d**, Schematic of a part of an AngioChip tissue. **e**–**g**, Scanning electron micrographs (SEMs) of a 1D tube (**e**; scale bars, 1.5 mm and 500 μm), a 2D AngioChip scaffold (**f**; scale bars, 1 mm and 300 μm) and a multi-layer 3D AngioChip scaffold with 20 μm micro-holes (**g**; scale bars, 1 mm and 400 μm) created using the 3D stamping technique. **h**, SEM of an AngioChip scaffold with 10 μm micro-holes on the channel walls. Scale bar, 200 μm. **i**,**j**, SEMs of the 3D lattice matrix in between the microchannels (**i**; scale bar, 100 μm) and the cross-section of a 10 μm micro-hole on the channel wall (**j**; scale bar, 50 μm). Red arrows point to the micro-holes. **k**,**l**, SEMs of the AngioChip scaffolds with 20 μm micro-holes on the top and side walls of the microchannels. Red arrows point to the micro-holes on the top and side walls. Scale bars, 400 μm (**k**), and 100 μm (**l**). **m**, Mass loss in one day from porogen leaching for pore-free and nanoporous AngioChip scaffolds (average ± s.d., $n=3$). Pore-free and nanoporous corresponds to scaffolds fabricated without or with the use of porogen, respectively. **n**, SEM of the surface of an AngioChip scaffold after porogen leaching. Scale bar, 500 nm.

biodegrades by hydrolysis[27] (Supplementary Figs 1 and 2); and is more elastic than FDA (Food and Drug Administration)-approved polyesters[29]. Citric acid-based elastomers also have low thrombogenicity[30,31]. Thin POMaC sheets were pre-patterned, in a scalable manner (Fig. 1a), under ultraviolet illumination and stamped onto each other, layer by layer with precise alignment down to several micrometres, to form complex suspended microstructures and internal cavities. POMaC exhibited temporary and differential adhesion to glass (strong) and polydimethylsiloxane (PDMS; weak) after photo-crosslinking, due to oxygen-induced inhibition of free radical polymerization on the surface of the PDMS (ref. 32), which leaves a non-polymerized POMaC layer at the interface. Patterned POMaC sheets were robustly transferred, aligned and released from one substrate (PDMS) and then bound to the POMaC structures supported by a glass substrate (Supplementary Fig. 3), circumventing the challenge of printing biomaterials in mid-air[33].

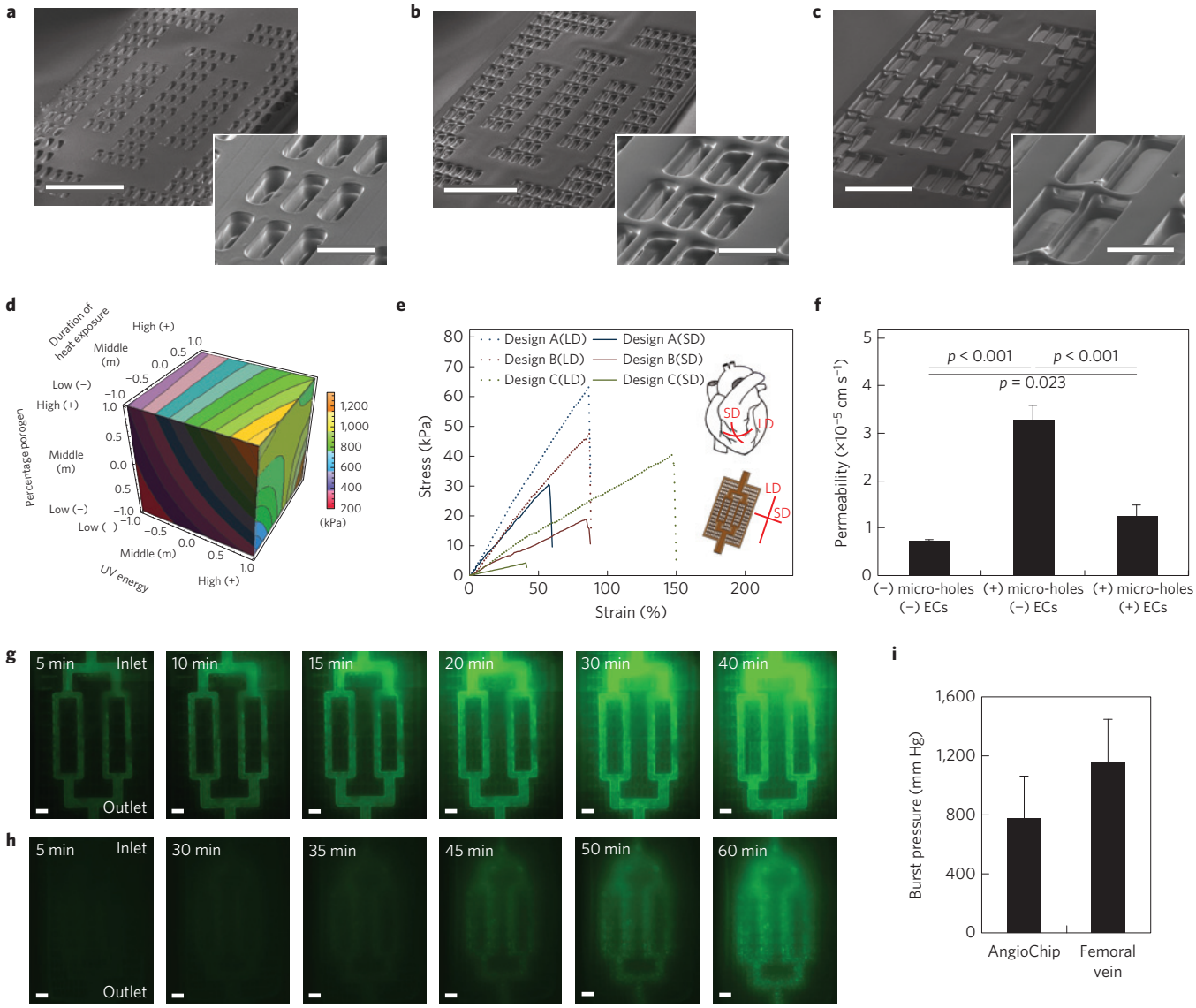


**Figure 2 | Physical characterization of the AngioChip scaffolds. a–c**, SEMs of the AngioChip scaffolds with lattice matrices of increasing macro-porosity: design A (**a**; scale bars, 1 mm and 200 μm), design B (**b**; scale bars, 1 mm and 200 μm), and design C (**c**; scale bars, 1 mm and 300 μm). **d**, Isosurface plot of the bulk elasticity of POMaC as a function of ultraviolet (UV) energy, heat exposure duration and percentage of porogen, evaluated at the citric acid to maleic anhydride monomer molar ratio of 1:4. **e**, Representative uniaxial tensile stress–strain plots of the AngioChip scaffolds with the three different lattice matrix designs. Long-edge direction (LD) and short-edge direction (SD) correspond to the circumferential and longitudinal axes of the heart, respectively ($n=3$). **f**, Permeability of AngioChip scaffold wall to FITC (fluorescein isothiocyanate)–dextran (70 kDa) with and without EC coating or 10 μm micro-holes (average ± s.d., $n=3$). **g**, Time-lapse fluorescent images of 332 Da FITC diffusing from the built-in network of an AngioChip scaffold with 10 μm micro-holes to the surrounding lattice matrix. Scale bars, 300 μm. Final images were stitched from multiple images. **h**, Time-lapse images of carboxyfluorescein diacetate (CFDA, 557 Da) diffusing from the built-in internal network with 10 μm micro-holes to the surrounding cardiac tissue where it is cleaved by the viable cells ($n=3$). Scale bars, 300 μm. **i**, Burst pressure of AngioChip scaffolds (average ± s.d., $n=4$) and rat femoral veins (average ± s.d., $n=6$).

3D stamping enabled patterning of POMaC into various intricate structures from a 1D tube (Fig. 1e) to 2D bifurcating conduits (Fig. 1f) or a 3D branching network (Fig. 1g) mimicking a vascular bed within a fully interconnected lattice matrix, tailored to support the parenchymal cells (Fig. 1c,d,f,g and Supplementary Fig. 4).

Internal networks branching in the $x$–$y$ as well as $y$–$z$ planes were perfusable through a single inlet and outlet (Fig. 1b,f,g and Supplementary Fig. 4 and Supplementary Movie 1). The smallest microchannel in the network was 100 μm by 50–100 μm, with a wall thickness of 25–50 μm. To improve the exchange of biomolecules and cell migration, 10 μm micro-holes were patterned in the upper channel walls (Fig. 1h–j and Supplementary Fig. 5a,b). To increase porosity, 20 μm micro-holes were patterned in the top and side channel walls (Fig. 1k,l and Supplementary Fig. 5c). To further enhance oxygen and nutrient exchange, nanopores were incorporated into the bulk polymer by embedding and subsequently leaching out a porogen, confirmed by mass reduction (Fig. 1m) and resulting in wrinkled nanopores, similar to described previously[34] (Fig. 1n).

For perfusion culture, the AngioChip scaffolds were installed in the main well between the inlet and outlet well of a customized bioreactor (Fig. 1c and Supplementary Fig. 6). Culture medium or endothelial cell (EC) suspension was perfused through the internal network driven by the liquid pressure-head differences (Fig. 1c and Supplementary Fig. 7). This design removed the need for pumps, allowing access to both the parenchymal space and the internal

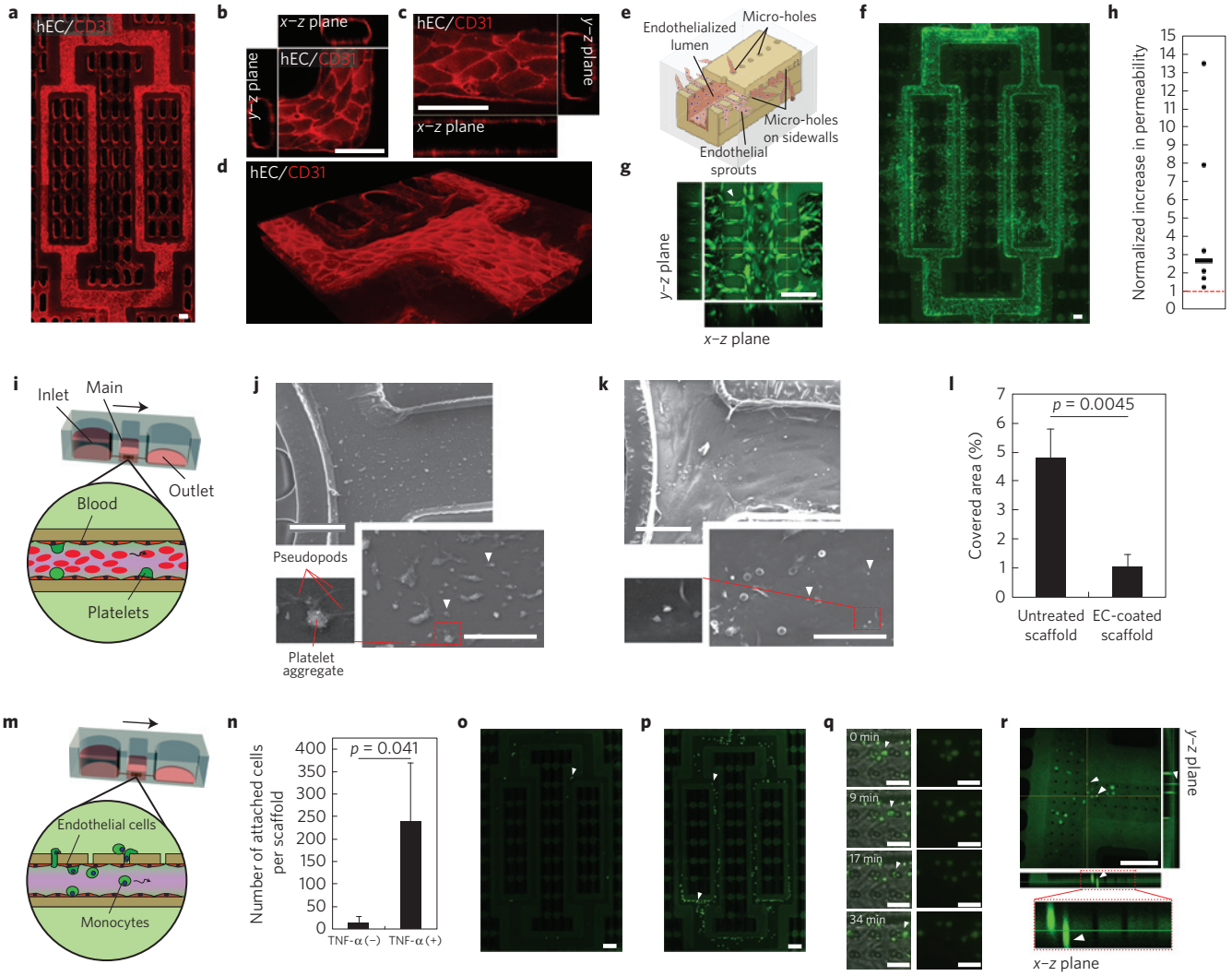


**Figure 3 | Endothelialization of the AngioChip network. a–d**, Immunostaining (CD31, red) of the internal vasculature of an AngioChip scaffold on day 2 with a view of the entire network (**a**; scale bar, 100 μm; image was stitched from multiple images), a view of a corner (**b**; scale bar, 100 μm), and a straight segment (**c**; scale bar, 100 μm), and a branch (**d**; $n=3$). **e**, Schematic of ECs migrating and sprouting from the inner lumen of the microchannel to the surrounding parenchyma through the built-in 20 μm micro-holes on the sidewalls. **f**,**g**, Fluorescent image of ECs (labelled green) sprouting from the channel networks into the parenchymal space on day 2 ($n=4$). White arrowhead points to a vessel sprouting within the micro-hole on the sidewall. Scale bars, 100 μm. **h**, Change in permeability of the endothelialized networks with 20 μm micro-holes to 70 kDa dextran on treatment with thymosin β4 for 24 h. Normalization was performed by dividing the permeability of the endothelium after Tβ4 application for 24 h by the unstimulated starting endothelium permeability of the same batch ($n=6$). **i**, Schematics of the human whole blood perfusion through the endothelialized AngioChip network. The AngioChip scaffold is located in the main well. The black arrow indicates the flow direction. **j**,**k**, SEMs of the luminal surface of an untreated scaffold network (**j**) and the luminal surface of an endothelialized network (day 2 in culture) after perfusion with 1% (v/v) heparinized human whole blood at 15 dyne $cm^{-2}$ for 30 min (**k**; $n=3$). Scale bars, 100 μm (**j**,**k**), and 50 μm (inset). White arrowheads point to representative platelets. **l**, Quantification of the luminal surface area of the scaffold network covered by the platelets (average ± s.d., $n=3$). **m**, Schematic of the perfusion of monocytes through the endothelialized network with 10 μm micro-holes. **n**, Quantification of adhered THP-1 monocytes on the inner luminal surface of an EC-coated AngioChip scaffold (day 2 in culture) with or without TNF-α treatment (average ± s.d, $n=3$). **o**,**p**, Images of fluorescently labelled THP-1 monocytes on an EC-coated AngioChip network without (**o**) or with (**p**) prior TNF-α treatment ($n=3$). Scale bars, 200 μm. White arrowheads point to adhered monocytes. **q**, Time-lapse images of fluorescently labelled monocytes (green) migrating laterally in the endothelialized scaffold network passing through a 10 μm micro-hole ($n=3$). Scale bars, 50 μm. **r**, Trans-endothelial migration of fluorescently labelled monocytes (green) through the 10 μm micro-holes on the channel wall ($n=3$). Scale bar, 200 μm. White arrowheads point to migrating monocytes.

vasculature using simple tools (for example, micropipettes), and enabling facile tissue removal (Fig. 1b). ECs were cultured within the internal network and the parenchymal cells were cultured within the lattice with native ECMs, allowing tissue remodelling (Fig. 1d).

## Tunable elasticity and permeability of AngioChips

The hydrolytically degradable scaffold lattice (Supplementary Fig. 8a,b) was composed of multiple layers of meshes in the parenchyma connected by vertical posts (50 μm diameter; Fig. 1i). This feature provided 100% interconnectivity (Fig. 1g), facilitating cell seeding and enabling formation of tissues in both the $x$–$y$ and $y$–$z$ plane. The Young's modulus of the adult human myocardium was reported to vary from 10–20 kPa (relaxed) to 200–500 kPa (contracted)[35–38], whereas for adult liver it varied from 0.6–2.0 kPa for healthy and up to 20 kPa for fibrotic livers[39]. By varying the ultraviolet and heat exposure, monomer ratio and porogen

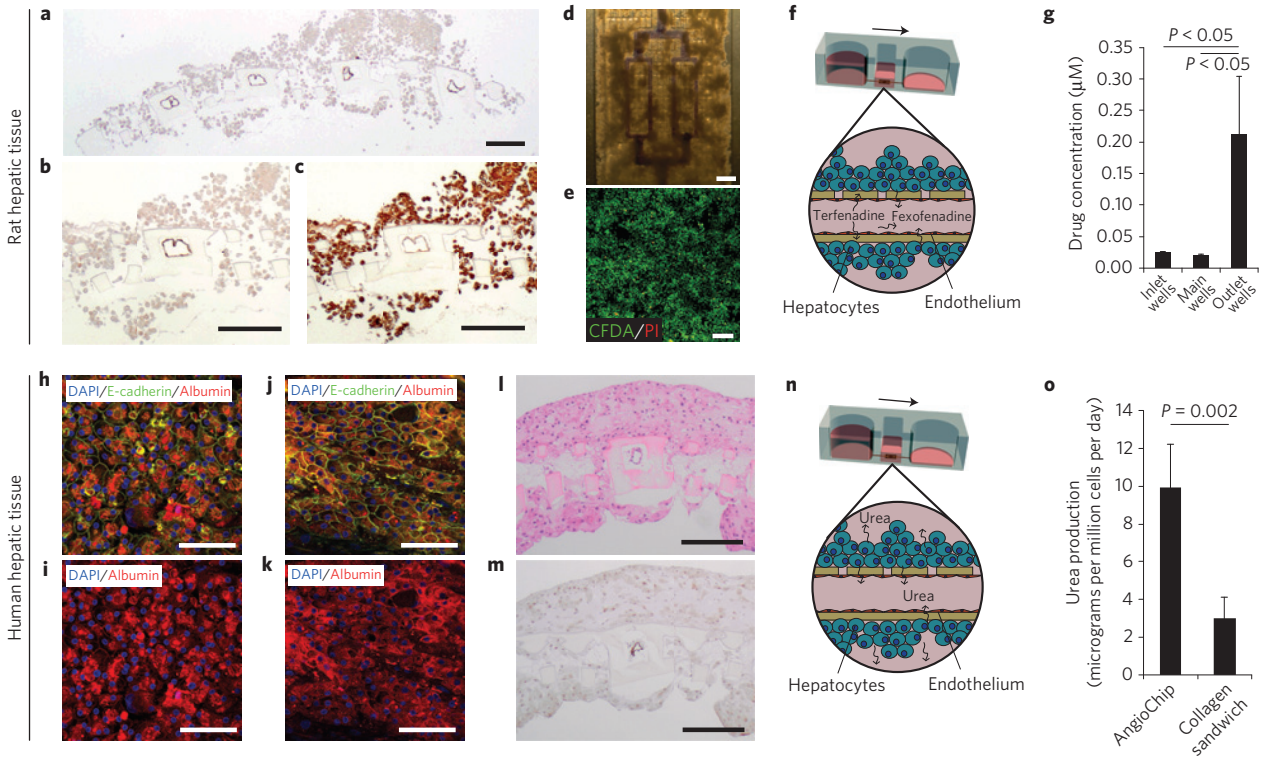


**Figure 4 | Vascularized hepatic tissue assembly. a–c**, Histology cross-section of hepatic tissue with 10 μm micro-holes on day 6 stained for CD31 to identify endothelial cells (**a**,**b**; $n=3$, scale bars, 200 μm) and albumin to identify hepatocytes (**c**; $n=3$, scale bar, 200 μm). **d**, Bright-field image of hepatic tissue perfused with blue colour dye. Scale bar, 500 μm. **e**, Fluorescent image of CFDA (green)- and propidium iodide (PI, red)-stained hepatic tissue shows high cell viability. Scale bar, 200 μm. **f**, Schematic of terfenadine diffusing through the vessel wall with 10 μm micro-holes into the hepatic tissue and then subsequently being converted into fexofenadine and released back into the vasculature. **g**, Concentration of fexofenadine in the bioreactor inlet, main and outlet wells after 24 h perfusion of terfenadine at 10 μM from inlet wells (average ± s.e.m., $n=4$) on day 3. **h–k**, Immunostaining of E-cadherin and albumin on a human hepatocyte monolayer collagen sandwich (**h**,**i**) and human AngioChip hepatic tissue (**j**,**k**) on day 7 ($n=3$). Scale bars, 100 μm. **l**,**m**, Histology cross-sections of human AngioChip hepatic tissues with 10 μm micro-holes on day 7 stained with haematoxylin and eosin (**l**), and for CD31 (**m**) to identify endothelial cells ($n=3$). Scale bars, 200 μm. **n**, Schematic of urea secretion from the hepatic tissue and release into the vasculature with 10 μm micro-holes. **o**, Quantification of urea secretion, normalized to cell number, into the bioreactor main well and outlet well from AngioChip hepatic tissue and collagen sandwich control on day 3 (average ± s.d., $n=4$).

concentration, we were able to achieve the Young's modulus of POMaC bulk polymer ranging from 53 ± 8 to 1,423 ± 651 kPa (Fig. 2d, Supplementary Fig. 8c and Supplementary Tables 1–4).

The geometry and density of the AngioChip parenchymal lattice were further varied to fine-tune the scaffold mechanical properties to resemble the anisotropic properties of the adult rat ventricular myocardium as in design B (Fig. 2a–c,e and Supplementary Figs 9 and 10 and Supplementary Table 5). Anisotropy was enabled by the rectangular shape of the mesh, with higher spatial density for struts oriented in the long-edge direction than in the short-edge direction (Fig. 2e). Both the effective elasticity and the ultimate tensile strength increased with lattice density. Further design iterations can yield scaffolds with mechanical properties tailored for specific applications (for example, human myocardium or human liver) by tuning the lattice structure and the elasticity of the base material (Fig. 2d).

The limited permeability of synthetic polymers hinders the success of other biodegradable microfluidic scaffolds[24,25]. Although some biocompatible polymers are permeable to $O_2/CO_2$ (ref. 40), they have a limited permeability for small molecules and proteins[41], necessitating introduction of porosity to enhance permeability (for example, as in Transwell membranes, $9.3 \times 10^{-5}$ cm s$^{-1}$ for 4 kDa molecules[42]). We found that the cell-free internal AngioChip network with 10 μm micro-holes was permeable to both small and large molecules (Fig. 2f,g). It was >4 times more permeable for large molecules (70 kDa TRITC–dextran) than the one without the 10 μm micro-holes, >2 times more permeable than EC-covered network and more permeable than mammalian venules and capillaries *in vivo* (Fig. 2f). The permeability of the EC-covered network was higher than the permeability of mammalian venules ($(0.15 \pm 0.05) \times 10^{-6}$ cm s$^{-1}$) for 70 kDa FITC–dextran[43] and comparable to that of capillaries[44] to proteins ($4.3 \times 10^{-6}$ cm s$^{-1}$). High permeability of the cell-free network allowed the EC coating to be the dominating transport resistance (Fig. 2f), similar to how the ECs govern the permeability of blood vessels *in vivo*. The live cell tracker dye, carboxyfluorescein diacetate (CFDA, 557 Da), was perfused through the network surrounded by cardiac cells, staining the live cells in the parenchyma (Fig. 2h), consistent with convection–diffusion transport and metabolic conversion within the tissue. There was no significant leakage of the culture medium during perfusion into the parenchymal space even in the absence of the endothelial cell coating (Supplementary Fig. 8d). The AngioChip burst pressure was comparable to that of the rat femoral vein (Fig. 2i and Supplementary Movie 2) and ~7-fold higher than the normal systolic blood pressure in a rat (130 mmHg) or a human (120 mmHg), indicating that the network will be sufficient to withstand blood perfusion in the peripheral circulation.

## Lumen endothelialization, sprouting and transmigration

On endothelialization with human umbilical vein ECs (HUVECs), CD31 immunostaining revealed a confluent endothelium on the luminal network surface (day 2, Fig. 3a–d and Supplementary

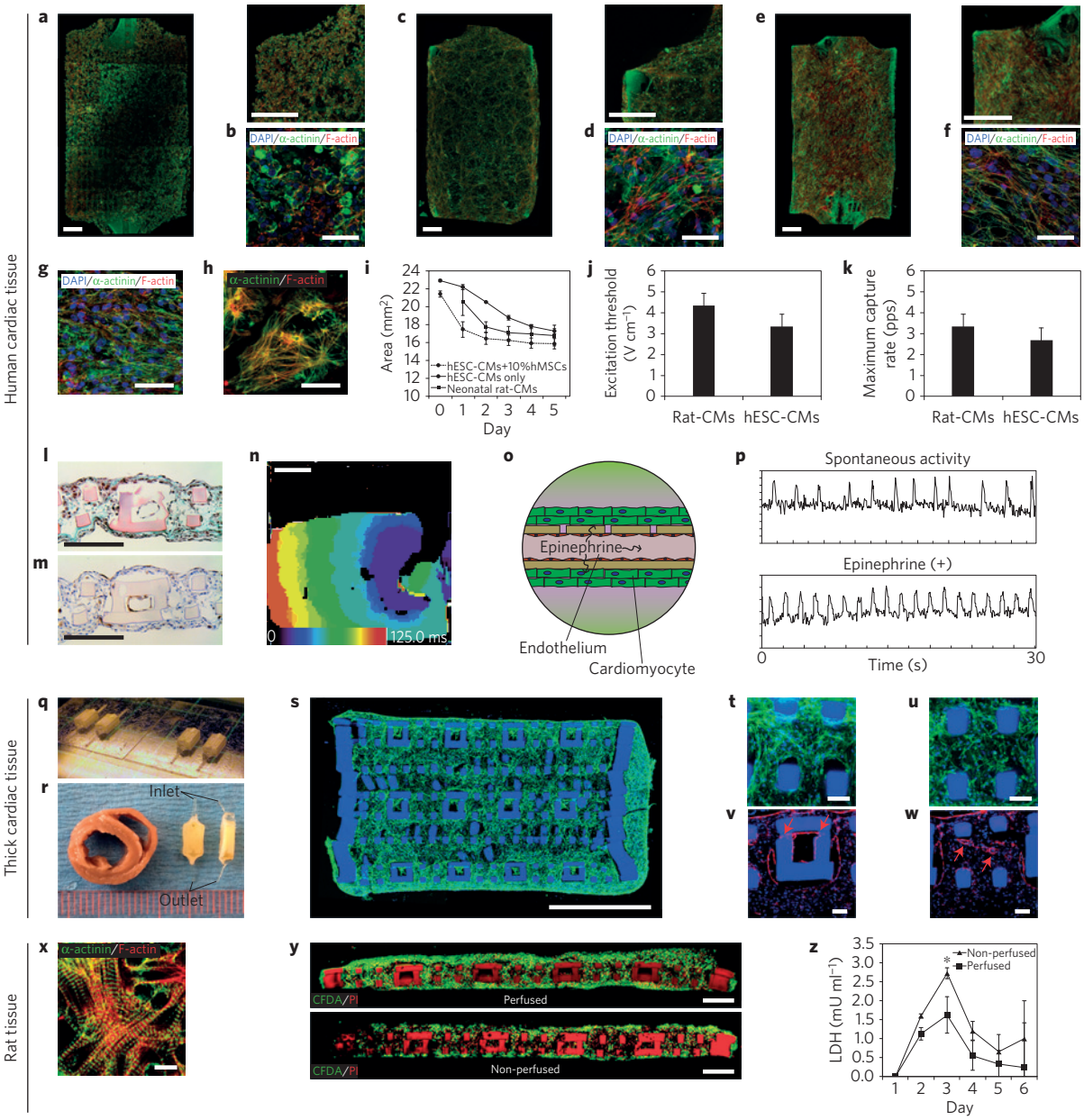


**Figure 5 | Vascularized cardiac tissue assembly. a**–**f**, Immunostaining of sarcomeric-α-actinin (green) and F-actin (red) on human AngioChip cardiac tissues with 10% human mesenchymal stem cells (hMSCs) on day 1 (**a**,**b**) and day 7 (**e**,**f**) or without hMSCs on day 7 (**c**,**d**) ($n=3$). Images directly above **b**,**d**,**f**, correspond to panels **a**,**c**,**e**, respectively. Scale bars, 500 μm (**a**,**c**,**e**), and 50 μm (**b**,**d**,**f**). In **a**,**c**,**e**, final images were stitched from multiple images. **g**,**h**, Immunostaining of sarcomeric-α-actinin (green) and F-actin (red) on Biowire platform (**g**) and monolayer (**h**) ($n=3$) on day 7. Scale bars, 50 μm. **i**, Quantification of decreasing tissue size due to cell remodelling for neonatal rat cardiomyocytes (rat-CMs), human embryonic stem cell-derived cardiomyocytes (hESC-CMs), and hESC-CMs mixed with 10% hMSCs (average ± s.d., $n=3$). **j**,**k**, Electrical excitability parameters (average ± s.d., $n=3$) on day 7. **l**,**m**, Histology cross-sections of human cardiac tissues on day 7 stained with Masson's trichrome (**l**), and for CD31 (**m**) to identify endothelial cells ($n=3$). Scale bars, 200 μm. **n**, Activation map of human AngioChip cardiac tissue on day 7 ($n=7$). Scale bar, 1 mm. Activation of the construct is seen from the stimulus point on the right propagating to the left over a time span of 100 ms, in a uniform manner. **o**, Schematic of perfusion delivery of the epinephrine drug through the built-in vasculature with 10 μm micro-holes. **p**, Initial spontaneous contraction trace and drug-stimulated contraction trace of a human cardiac tissue on day 7 perfused with 10 μM epinephrine ($n=3$). **q**, Image of multiple thick AngioChip scaffolds patterned in parallel on glass slides. **r**, Image of two thick AngioChip cardiac tissues placed face up and side up beside a slice of an adult rat heart. Scale shown in millimetres. **s**–**u**, Immunostaining of F-actin (green) of the cross-section of an endothelialized thick multi-layer human AngioChip cardiac tissue with 20 μm micro-holes on day 3 based on fibrin gel and hESC-derived CMs ($n=3$). In **s**, the final image was stitched from multiple images. Panels **t**,**u** show high-magnification images of tissue fibres in the parenchymal space near the edge region (**t**) and the centre region (**u**). Scale bars, 1 mm (**s**), and 50 μm (**t**,**u**). **v**,**w**, Immunostaining of CD31 of an endothelialized microchannel lumen with 20 μm micro-holes that guide sprouting (red arrows; **v**) and an adjacent parenchymal space with self-assembled microvasculature (red arrows; **w**) in a thick multi-layer human AngioChip cardiac tissue on day 3 ($n=3$). Scale bars, 50 μm (**v**,**w**). **x**, Immunostaining of sarcomeric-α-actinin (green) and F-actin (red) on a rat AngioChip cardiac tissue on day 7. Scale bar, 10 μm. **y**, CFDA (green)- and PI (red)-stained images of the cross-section of rat cardiac tissues with 10 μm micro-holes cultivated with or without medium perfusion on day 7 ($n=3$). Scaffold also stains red. Scale bars, 200 μm. Final images were stitched from multiple images. **z**, Quantification of lactate dehydrogenase (LDH) secretion from rat cardiac tissues cultivated with or without medium perfusion (average ± s.d., $n=4$). *, significant difference between groups with $p<0.05$.

Fig. 11a–c, day 7 Supplementary Fig. 11e–h) with VE-cadherin expressed at the cell–cell junctions (day 2, Supplementary Fig. 11d). The ECs physically covered the micro-holes on the vessel wall (Fig. 3b,c and Supplementary Fig. 11a–c), conformally and confluently coating the lumen even at the branch points (Supplementary Movie 3). In response to an angiogenic stimulus, thymosin β4, ECs migrated through the 20 μm micro-holes into the parenchymal space, a first step of angiogenesis (Fig. 3e–g). Endothelial network permeability dynamically increased in response to this biological stimulus (Fig. 3h), a feature unique to living cells that cannot be reproduced using the polymer material alone. Human whole blood was perfused through the AngioChip network with or without EC coating at 15 dyne $cm^{-2}$ (~5 μl $min^{-1}$; Re, 0.023; Fig. 3i). The AngioChip network was designed so that the ECs in the first- and second-order branches experienced the same shear stress. Without an EC coating, more platelets bound to the network surface (Fig. 3i–l and Supplementary Fig. 12) and became activated, as indicated by their extended pseudopodal morphology (Fig. 3j). Attached platelets exhibited a trend to spread according to the blood flow pattern and accumulated more at the stagnation regions of branches and turns (Fig. 3j and Supplementary Fig. 12). Perfused human monocytes, THP-1, exhibited accumulation and adhesion in the network in response to an inflammatory stimulus, TNF-α (Fig. 3m–p), subsequent migration along the endothelialized surface (Fig. 3q) and transmigration through the 10 μm micro-holes on the vessel walls, into the parenchymal space (Fig. 3r). The AngioChip was versatile enough to also enable migration of Raw264.7 macrophages (Supplementary Fig. 13).

## Urea secretion and drug metabolism in vascularized liver

Primary rat hepatocytes mixed with 10% primary rat fibroblasts (to facilitate ECM remodelling and gel compaction[9]) were seeded into the parenchymal space of an endothelialized AngioChip scaffold, resulting in the aggregation of viable cells (Fig. 4a–e and Supplementary Fig. 14a). Hepatocytes (albumin stained) distributed throughout the lattice and around the vessel network, and ECs (CD31 stained) coated the inner lumen of the network (Fig. 4a–c). Hepatic tissues were challenged with terfenadine, an antihistamine withdrawn from the market owing to cardio-toxicity[45] (Fig. 4f,g). Terfenadine is generally metabolized in the liver, to non-cardio-toxic fexofenadine, by the enzyme cytochrome P450 CYP3A4 isoform[45]. Liquid chromatography–mass spectrometry revealed the presence of fexofenadine in the outlet well (Fig. 4g).

Entirely human liver AngioChips were engineered using human embryonic stem cell (hESC)-derived hepatocytes[46], human mesenchymal stem cells (hMSCs) as a supporting population and

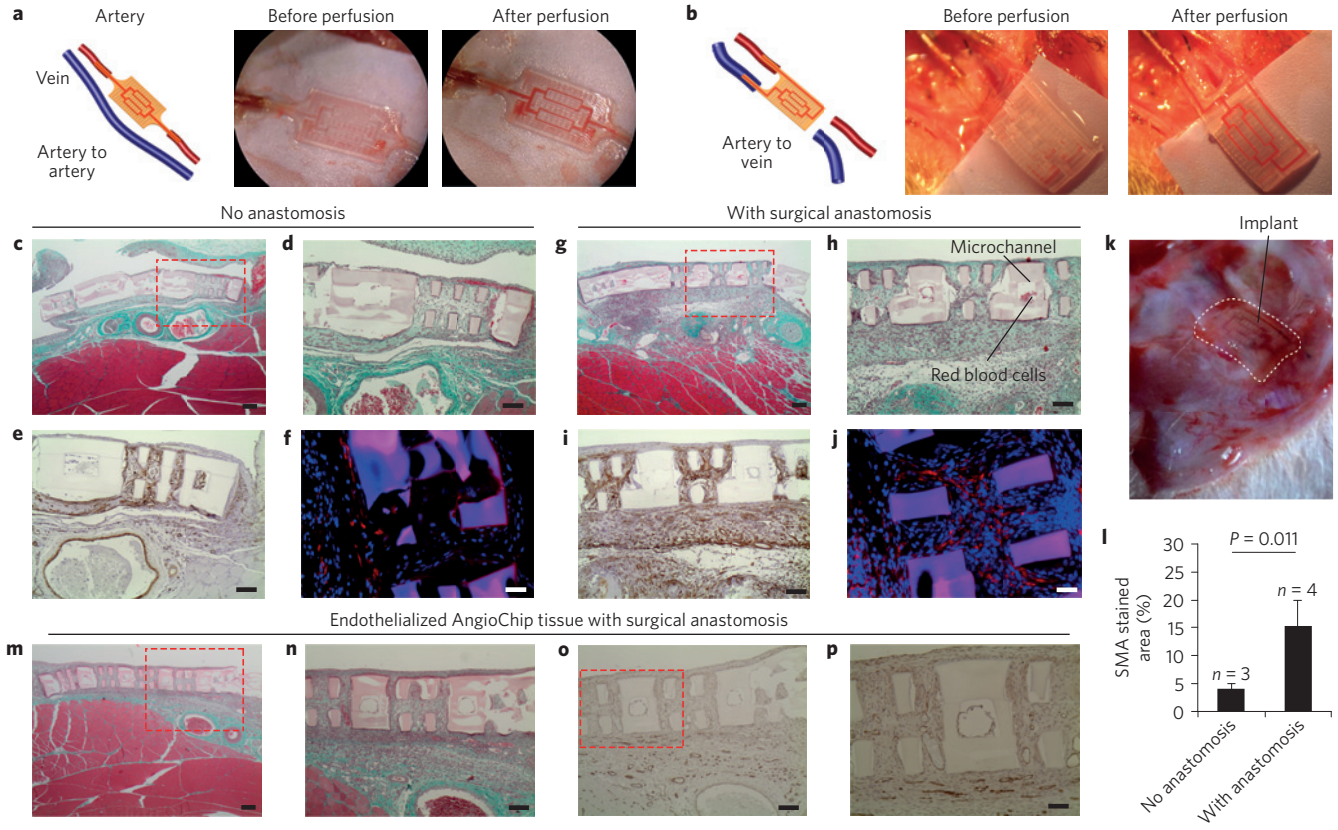


**Figure 6 | Surgical anastomosis of the cardiac tissue. a**,**b**, Surgical anastomosis of the AngioChip cardiac tissue on the rat femoral vessels in the configuration of artery-to-artery graft (**a**) and artery-to-vein graft (**b**). Blood perfusion was established immediately after anastomosis. Papers were placed under the implants during imaging for better visual contrast. **c**–**j**, Cross-section of the non-endothelialized rat cardiac tissue implants 1 week after surgery without (**c**–**f**; $n=3$) or with direct anastomosis (**g**–**j**; $n=4$) in the configuration of artery-to-vein graft. The sections were stained with Masson's trichrome (**c**,**d**,**g**,**h**), for smooth muscle actin (**e**,**i**), and for troponin T (**f**,**j**; red). Scale bars, 200 μm (**c**,**g**), 100 μm (**d**,**e**,**h**,**i**) and 50 μm (**f**,**j**). **k**, Image of a cardiac tissue implant on rat hindlimb 1 week after surgery with direct anastomosis in the configuration of artery-to-vein graft. White dotted line outlines the AngioChip implant. **l**, Quantification of the area stained for smooth muscle actin (average ± s.d.). **m**–**p**, Histology cross-sections of an AngioChip cardiac tissue endothelialized with Lewis rat primary vein endothelial cells and implanted with direct surgical anastomosis after 1 week ($n=3$). The sections were stained with Masson's trichrome (**m**,**n**), and for CD31 (**o**,**p**). Scale bars, 200 μm (**m**), 100 μm (**n**,**o**) and 50 μm (**p**). Red dashed boxes in **c**,**g**,**m**,**o** indicate the imaging location of panels **d**,**h**,**n**,**p**, respectively.

HUVECs for inner lumen coating. High-density culture resulted in the formation of junctions between hepatocytes (Fig. 4j), positive staining for albumin (Fig. 4k) and bile canaliculi (Supplementary Fig. 15), which were similar in appearance to those obtained from a collagen sandwich (Fig. 4h,i), a commonly used control. Cell density was $0.6 \pm 0.2 \times 10^8$ cells cm$^{-3}$ at day 7 with cells present throughout the AngioChip volume and CD31$^+$ ECs coating the inner lumen (Fig. 4l,m). Secretion of urea per cell from endothelialized AngioChip tissues was quantified and shown to be higher than that of the collagen sandwich control (Fig. 4n,o).

## Scalable assembly of vascularized cardiac tissue

Cardiac tissues were created from either hESC-derived (Fig. 5a–w and Supplementary Figs 14b and 18) or neonatal rat cardiomyocytes (Fig. 5x–z). To provide evidence of tissue-level organization, entire AngioChips based on entirely human cells (hESC-derived cardiomyocytes, 10% hMSCs and HUVECs) were imaged using confocal microscopy. Elongated cell bundles were present throughout the entire volume (Fig. 5a–f and Supplementary Fig. 14b) including the scaffold interior (Fig. 5l,m and Supplementary Fig. 16). Although gel compaction was possible without the addition of supporting cells, tissues were more compacted and aligned when 10% MSCs was used (Fig. 5c,e). Cardiac cell density, estimated from the histology sections, was $2.3 \pm 0.8 \times 10^8$ cells cm$^{-3}$. A condensed tissue formed within 5 days (Fig. 5i and Supplementary Figs 14b and 16); a time frame consistent with previously published studies of non-vascularized cardiac tissues that relied on gel compaction (5 days for human[5] and 7 days for rat[47]). Synchronous macroscopic contractions were observed as early as day 4 and the electrical excitability parameters of both rat and human tissues fell within the standard range for non-vascularized rat constructs[48] and both rat[9,47] and human micro-tissues[5] (Fig. 5j,k). AngioChip cardiac tissues contracted macroscopically and compressed the scaffold at each beat (Supplementary Fig. 17b) without collapsing the internal vessel network while being perfused (Supplementary Movies 4 and 5). The contractile protein sarcomeric α-actinin and the structural protein F-actin were visible in the elongated cells (Fig. 5d,f and Supplementary Fig. 16). Striated cardiac tissue bundles of the AngioChip were similar to those present in the 3D Biowire construct, a control that previously improved cardiomyocyte structural maturation[5] (Fig. 5g). Cardiomyocytes cultivated in monolayers, a standard control, exhibited cross-striations, but a lack of overall orientation and a less anisotropic overall structure (Fig. 5h) compared with those cultured in AngioChips (Fig. 5f). At day 7, ECs coated the vessel lumen, and cardiomyocytes distributed throughout the lattice and packed around the vessels (Fig. 5l,m). Human cardiac tissue exhibited impulse propagation across the entire tissue ($4.8 \pm 1.3$ cm s$^{-1}$, $n = 7$), without conduction block (Fig. 5n and Supplementary Movie 6). These values are lower than conduction velocities (voltage) we reported for Biowires previously[5], as AngioChips were cultivated for a shorter period of time and without electrical stimulation. Conduction velocity can be further improved by electromechanical stimulation[5,49]. Within 30–40 min of application, the tissues showed the expected positive chronotropic response to epinephrine (10 μM, Fig. 5o,p and Supplementary Fig. 17a).

Engineering millimetre-scale thick tissues was possible using two scalable approaches: by fabricating multi-layer scaffolds (1.58 mm thick, Fig. 5q and Supplementary Fig. 20a) using the 3D stamping technique with one inlet and one outlet (Fig. 5q–w and Supplementary Fig. 20); or by stacking individual single-layer AngioChip tissues followed by cultivation under perfusion to create a single multi-layer thick tissue with multiple inlets and outlets (Supplementary Fig. 19). Fibrin gel or Matrigel hydrogel was independently used, demonstrating versatility of hydrogel choices for parenchymal cell seeding. The resulting cardiac tissue was 1.75–2 mm thick with a high density of elongated cells throughout the cross-section (Fig. 5s–u and Supplementary Fig. 20g,h) and visible cross-striations in the cells from the scaffold interior even after only 3 days in culture (Supplementary Fig. 20i). Although the tissue was based on human cardiomyocytes, it was comparable to the thickness of a physiological structure, the adult rat heart left ventricle (Fig. 5r).

The inner lumen of the AngioChip scaffold in the thick tissues was fully endothelialized, with organization of endothelial tubule-like structures in the parenchymal space to provide an additional level of vascularization (Fig. 5v,w and Supplementary Fig. 20f,j–l). In some instances, these tubular structures clearly connected with the endothelial cells sprouting, through the 20 μm micro-holes, from the inner luminal structures of the AngioChip scaffolds (Supplementary Fig. 20f,j–l), demonstrating the direct interaction of the cells in the two compartments.

Rat cardiac tissue (Fig. 5x) exhibited higher viability under perfusion compared with the non-perfused controls, which developed a necrotic core at day 7 (Fig. 5y). Most cell death (that is, lactate dehydrogenase release) occurred within the first 3 days and medium perfusion helped mitigate cell death (Fig. 5z) on day 3, clearly demonstrating the benefit of perfusion even for the single-layer AngioChip tissues.

## Surgical anastomosis of AngioChips to host vasculature

AngioChip scaffolds were connected to the femoral vessels on the hindlimbs of adult Lewis rats, in artery-to-artery (Fig. 6a) and artery-to-vein (Fig. 6b) mode, to demonstrate two different configurations of direct surgical anastomosis. The inlet and outlet (inner dimensions of 100 μm × 200 μm and outer dimensions of 300 μm × 400 μm) were connected to femoral vessels (Fig. 6) with surgical cuffs. Similar citric acid-based polymers[28] have been shown to be antithrombotic in vascular grafts and to support EC growth *in vivo*[30,31]. The animals were heparinized only during surgery. In both configurations, blood perfusion was established immediately, even in the absence of ECs (Fig. 6a,b), although artery-to-artery mode was more technically challenging owing to the higher pressure (Supplementary Movie 7). Blood pulsation was also observed (Supplementary Movie 7), more noticeably in the artery-to-artery configuration. Erythrocytes were observed only in the networks of tissues implanted with direct anastomosis (Fig. 6c,d,g,h,k and Supplementary Figs 21 and 22). One week after the implantation of the AngioChip cardiac tissues, native angiogenesis also took place around the implants (Supplementary Fig. 23). The presence of smooth muscle actin (SMA)-positive cells was merely 2% in the isolated neonatal rat heart cells[4]; the significant SMA staining (Fig. 6e,i and Supplementary Fig. 24) suggested the penetration of mural cells or myofibroblasts into the implanted tissues consistent with the healing response[50] (Fig. 6l). Troponin T immunostaining demonstrated some elongated cardiomyocytes intertwining within the lattice of the AngioChips (Fig. 6f,j and Supplementary Fig. 25). AngioChip cardiac tissues endothelialized with Lewis rat primary vein ECs were also implanted with direct anastomosis in the artery-to-vein configuration. One week later, ECs coating the lumen were observed in 50% of the microchannels from three different implants (2/5, 4/5, 1/5 of visible lumen for implant 1, 2, 3, respectively; Fig. 6m–p). Histologically, 85% of AngioChip lumen were blood clot free after 1 week *in vivo* (Supplementary Figs 21 and 22). Specifically, in non-EC-coated AngioChips 3/3, 3/3, 4/5 and 3/5 of visible lumens were blood clot free in the four implants and in the EC-coated groups 3/5, 5/5 and 5/5 were blood clot free in the three implants. The channel walls did not degrade appreciably in one week, indicating that a longer time is required, as biodegradation and biocompatibility studies showed POMaC polymer discs persisted for at least 5 weeks *in vivo* (Supplementary Fig. 26).

## Outlook

AngioChip provides a powerful platform technology for cultivation of vascularized tissues that overcomes key limitations in the fields of tissue engineering (scalable production of millimetre-sized tissues), organ-on-a-chip engineering (precise placement of endothelial and parenchymal cells, in a simple to operate format) and *in vivo* tissue implantation (direct anastomosis). This technology does away with the requirement that cells be in direct contact with drug-absorbent PDMS in closed-channel systems for organs-on-chips, and does not solely rely on hydrogels as cell carriers, as these are typically too fragile to surgically connect into the hosts' circulation for *in vivo* implantation. Instead, AngioChip effectively decouples the material choice for the engineered vessel network from the material choice for the parenchymal space, allowing us to control the initial architecture of the vasculature and establish immediate perfusion *in vitro* and *in vivo* while sustaining the extensive remodelling of parenchyma. This micro-engineering approach provided no delay for tissue endothelialization, as a perfusable endothelial network was achieved within one day, before parenchymal cell seeding. The new 3D stamping technique allowed us to handle polymer sheets as thin as 25 μm with 10–20 μm holes to create a vessel wall that is merely 2–3 cells thick. Thus, paracrine signalling between the ECs and the parenchyma, which usually decays significantly within a very short distance (~10 cells)[51], can be sustained.

The thin channel walls in combination with the nanopores and micro-holes were the key features that allowed effective molecular exchange, cell extravasation in a vascularized 3D tissue model, and physiologically relevant modes for delivery of test drugs by convection–diffusion. The addition of 10 μm micro-holes covering only 0.5% of the total network surface area increased the permeability of the network by more than four times compared with the micro-hole-free scaffolds. The resulting permeability was higher than that of the native vasculature for EC-free AngioChips, ensuring that the polymer wall did not inhibit transport and enabling subsequent EC coating to act as a governing resistance. AngioChip networks with 20 μm micro-holes in the top and sidewalls increased the coverage of micro-holes to 3.2% of the surface area and guided the endothelial sprouts into the parenchyma. To further fine-tune the vessel permeability to match the unique environment in different organs, organ-specific ECs should be used. AngioChip also enables fine-tuning of the elasticity for specific organs, a factor important for preventing long-term inflammation and fibrosis[52], using a rectangular (for anisotropic[53]) or square (for isotropic[54]) lattice in the parenchymal space, difficult to achieve with hydrogels[21].

The AngioChip platform enables facile integration of different tissues on a single device by linking multiple AngioChips in series (Supplementary Fig. 27). Conventional microfluidic systems require bulky external set-ups that make integration difficult. Closed chip configuration is incompatible with the current practices in biological laboratories and the pharmaceutical industry, which rely heavily on open access for liquid dispensing with micropipetting. Our platform, resembling a standard multi-well plate, maintains an open configuration so that both the parenchymal space and the internal vasculature can be accessed with pipetting and allows different media to be used in each compartment, thus facilitating co-culture.

Long-term patency of the AngioChip networks should be determined in future *in vivo* studies. Immobilization of heparin onto the inner luminal surface with existing methods[50,55,56] could also enhance long-term blood vessel patency. Appropriate scaffold degradation rate is critical[50]; therefore, long-term degradation of the AngioChip *in vivo* should be examined in the future and fine-tuned for a specific application by adjusting the citric acid content on the polymer chain[27] to enable native mural cells and ECM to gradually take over the role of the synthetic polymer vessel wall. Future studies should determine whether the original blood vessels will remain, on complete AngioChip biodegradation, and whether the endothelialized vasculature will exhibit appropriate vasodilation and vasoconstriction properties *in vivo*. Other non-thrombogenic, photo-crosslinkable scaffold materials, with tissue-specific elasticity, could be explored. Electrical stimulation during cardiac culture on AngioChips should be used to further synchronize tissue contractions and mature cells[5]. The proof of concept for the use of AngioChip in organ-on-a-chip engineering provided here opens the door for future studies aimed at answering complex biological questions *in vitro* and *in vivo*.

In summary, the AngioChip was used to generate both *in vitro* cardiac and hepatic tissue models with defined vasculature and *in vivo* implants with direct surgical anastomosis. Uniquely, this platform could enable direct and rapid translation of *in vitro* testing results to *in vivo* validation and the development of effective regenerative strategies.

## Methods

Methods and any associated references are available in the online version of the paper.

Received 8 July 2014; accepted 19 January 2016; published online 7 March 2016

## References


1. Huh, D. *et al*. Reconstituting organ-level lung functions on a chip. *Science* **328,** 1662–1668 (2010).
2. Kim, H. J., Huh, D., Hamilton, G. & Ingber, D. E. Human gut-on-a-chip inhabited by microbial flora that experiences intestinal peristalsis-like motions and flow. *Lab Chip* **12,** 2165–2174 (2012).
3. Kolesky, D. B. *et al*. 3D bioprinting of vascularized, heterogeneous cell-laden tissue constructs. *Adv. Mater.* **26,** 3124–3130 (2014).
4. Zimmermann, W.-H. *et al*. Engineered heart tissue grafts improve systolic and diastolic function in infarcted rat hearts. *Nature Med.* **12,** 452–458 (2006).
5. Nunes, S. S. *et al*. Biowire: a platform for maturation of human pluripotent stem cell-derived cardiomyocytes. *Nature Methods* **10,** 781–787 (2013).
6. Yang, X., Pabon, L. & Murry, C. E. Engineering adolescence maturation of human pluripotent stem cell-derived cardiomyocytes. *Circ. Res.* **114,** 511–523 (2014).
7. Bian, W., Badie, N., Himel IV, H. D. & Bursac, N. Robust T-tubulation and maturation of cardiomyocytes using tissue-engineered epicardial mimetics. *Biomaterials* **35,** 3819–3828 (2014).
8. Takebe, T. *et al*. Vascularized and functional human liver from an iPSC-derived organ bud transplant. *Nature* **499,** 481–484 (2013).
9. Thavandiran, N. *et al*. Design and formulation of functional pluripotent stem cell-derived cardiac microtissues. *Proc. Natl Acad. Sci. USA* **110,** E4698–E4707 (2013).
10. Legant, W. R. *et al*. Microfabricated tissue gauges to measure and manipulate forces from 3D microtissues. *Proc. Natl Acad. Sci. USA* **106,** 10097–10102 (2009).
11. Bian, W. Engineered skeletal muscle tissue networks with controllable architecture. *Biomaterials* **30,** 1401–1412 (2009).
12. Kim, S., Lee, H., Chung, M. & Jeon, N. L. Engineering of functional, perfusable 3D microvascular networks on a chip. *Lab Chip* **13,** 1489–1500 (2013).
13. Zheng, Y. *et al*. *In vitro* microvessels for the study of angiogenesis and thrombosis. *Proc. Natl Acad. Sci. USA* **109,** 9342–9347 (2012).
14. Zhang, B., Peticone, C., Murthy, S. K. & Radisic, M. A standalone perfusion platform for drug testing and target validation in micro-vessel networks. *Biomicrofluidics* **7,** 044125 (2013).
15. Atala, A., Kasper, F. K. & Mikos, A. G. Engineering complex tissues. *Sci. Transl. Med.* **4,** 160rv112 (2012).
16. Bae, H. *et al*. Building vascular networks. *Sci. Transl. Med.* **4,** 160ps123 (2012).
17. Ye, L., Zimmermann, W.-H., Garry, D. J. & Zhang, J. Patching the heart cardiac repair from within and outside. *Circ. Res.* **113,** 922–932 (2013).
18. Baranski, J. D. *et al*. Geometric control of vascular networks to enhance engineered tissue integration and function. *Proc. Natl Acad. Sci. USA* **110,** 7586–7591 (2013).
19. Sekine, H. *et al*. *In vitro* fabrication of functional three-dimensional tissues with perfusable blood vessels. *Nature Commun.* **4,** 1399 (2013).
20. Shandalov, Y. *et al*. An engineered muscle flap for reconstruction of large soft tissue defects. *Proc. Natl Acad. Sci. USA* **111,** 6010–6015 (2014).
21. Miller, J. S. *et al*. Rapid casting of patterned vascular networks for perfusable engineered three-dimensional tissues. *Nature Mater.* **11,** 768–774 (2012).

22. Vollert, I. *et al*. *In-vitro* perfusion of engineered heart tissue through endothelialized channels. *Tissue Eng.* **20,** 854–863 (2013).
23. Tang, M. D., Golden, A. P. & Tien, J. Fabrication of collagen gels that contain patterned, micrometer-scale cavities. *Adv. Mater.* **16,** 1345–1348 (2004).
24. Ye, X. *et al*. A biodegradable microvessel scaffold as a framework to enable vascular support of engineered tissues. *Biomaterials* **34,** 10007–10015 (2013).
25. Bettinger, C. J. *et al*. Three-dimensional microfluidic tissue-engineering scaffolds using a flexible biodegradable polymer. *Adv. Mater.* **18,** 165–169 (2006).
26. Bettinger, C. J. *et al*. Silk fibroin microfluidic devices. *Adv. Mater.* **19,** 2847–2850 (2007).
27. Tran, R. T. *et al*. Synthesis and characterization of a biodegradable elastomer featuring a dual crosslinking mechanism. *Soft Matter* **6,** 2449–2461 (2010).
28. Yang, J., Webb, A. R. & Ameer, G. A. Novel citric acid-based biodegradable elastomers for tissue engineering. *Adv. Mater.* **16,** 511–516 (2004).
29. Spiller, K., Freytes, D. & Vunjak-Novakovic, G. Macrophages modulate engineered human tissues for enhanced vascularization and healing. *Ann. Biomed. Eng.* **43,** 616–627 (2014).
30. Kibbe, M. R. *et al*. Citric acid-based elastomers provide a biocompatible interface for vascular grafts. *J. Biomed. Mater. Res. A* **93A,** 314–324 (2010).
31. Motlagh, D. *et al*. Hemocompatibility evaluation of poly(diol citrate) *in vitro* for vascular tissue engineering. *J. Biomed. Mater. Res. A* **82A,** 907–916 (2007).
32. Dendukuri, D., Pregibon, D. C., Collins, J., Hatton, T. A. & Doyle, P. S. Continuous-flow lithography for high-throughput microparticle synthesis. *Nature Mater.* **5,** 365–369 (2006).
33. Derby, B. Printing and prototyping of tissues and scaffolds. *Science* **338,** 921–926 (2012).
34. Hoshi, R. A. Nanoporous biodegradable elastomers. *Adv. Mater.* **21,** 188–192 (2009).
35. Nagueh, S. F. *et al*. Altered titin expression, myocardial stiffness, and left ventricular function in patients with dilated cardiomyopathy. *Circulation* **110,** 155–162 (2004).
36. Weis, S. M. *et al*. Myocardial mechanics and collagen structure in the osteogenesis imperfecta murine (oim). *Circ. Res.* **87,** 663–669 (2000).
37. Coirault, C. *et al*. Increased compliance in diaphragm muscle of the cardiomyopathic Syrian hamster. *J. Appl. Physiol.* **85,** 1762–1769 (1998).
38. Omens, J. H. Stress and strain as regulators of myocardial growth. *Prog. Biophys. Mol. Biol.* **69,** 559–572 (1998).
39. Yeh, W. C. *et al*. Elastic modulus measurements of human liver and correlation with pathology. *Ultrasound Med. Biol.* **28,** 467–474 (2002).
40. Merkel, T. C., Bondar, V. I., Nagai, K., Freeman, B. D. & Pinnau, I. Gas sorption, diffusion, and permeation in poly(dimethylsiloxane). *J. Polym. Sci. B* **38,** 415–434 (2000).
41. Toepke, M. W. & Beebe, D. J. PDMS absorption of small molecules and consequences in microfluidic applications. *Lab Chip* **6,** 1484–1486 (2006).
42. Gaillard, P. J. *et al*. Establishment and functional characterization of an *in vitro* model of the blood-brain barrier, comprising a co-culture of brain capillary endothelial cells and astrocytes. *Eur. J. Pharm. Sci.* **12,** 215–222 (2001).
43. Yuan, W., Lv, Y., Zeng, M. & Fu, B. M. Non-invasive measurement of solute permeability in cerebral microvessels of the rat. *Microvasc. Res.* **77,** 166–173 (2009).
44. Adamson, R. H., Huxley, V. H. & Curry, F. E. Single capillary permeability to proteins having similar size but different charge. *Am. J. Physiol.* **254,** H304–H312 (1988).
45. Woosley, R. L., Chen, Y., Freiman, J. P. & Gillis, R. A. Mechanism of the cardiotoxic actions of terfenadine. *JAMA* **269,** 1532–1536 (1993).
46. Ogawa, S. *et al*. Three-dimensional culture and cAMP signaling promote the maturation of human pluripotent stem cell-derived hepatocytes. *Development* **140,** 3285–3296 (2013).
47. Boudou, T. *et al*. A microfabricated platform to measure and manipulate the mechanics of engineered cardiac microtissues. *Tissue Eng. A* **18,** 910–919 (2012).
48. Radisic, M. *et al*. Functional assembly of engineered myocardium by electrical stimulation of cardiac myocytes cultured on scaffolds. *Proc. Natl Acad. Sci. USA* **101,** 18129–18134 (2004).
49. Tulloch, N. L. *et al*. Growth of engineered human myocardium with mechanical loading and vascular coculture. *Circ. Res.* **109,** 47–59 (2011).
50. Wu, W., Allen, R. A. & Wang, Y. Fast-degrading elastomer enables rapid remodeling of a cell-free synthetic graft into a neoartery. *Nature Med.* **18,** 1148–1153 (2012).
51. Bhatia, S., Balis, U., Yarmush, M. & Toner, M. Effect of cell–cell interactions in preservation of cellular phenotype: cocultivation of hepatocytes and nonparenchymal cells. *FASEB J.* **13,** 1883–1900 (1999).
52. Mazza, E. & Ehret, A. E. Mechanical biocompatibility of highly deformable biomedical materials. *J. Mech. Behav. Biomed. Mater.* **48,** 100–124 (2015).
53. Engelmayr, G. C. *et al*. Accordion-like honeycombs for tissue engineering of cardiac anisotropy. *Nature Mater.* **7,** 1003–1010 (2008).
54. Nava, A., Mazza, E., Furrer, M., Villiger, P. & Reinhart, W. *In vivo* mechanical characterization of human liver. *Med. Image Anal.* **12,** 203–216 (2008).
55. Hoshi, R. A. *et al*. The blood and vascular cell compatibility of heparin-modified ePTFE vascular grafts. *Biomaterials* **34,** 30–41 (2013).
56. Sefton, M. V., Gemmell, C. H. & Gorbet, M. B. in *Biomaterials Science* 3rd edn (eds Ratner, B. D., Hoffman, A. S., Schoen, F. J. & Lemons, J. E.) 758–760 (Academic, 2013).


## Acknowledgements

We thank K. Marjan and P. Lai from the University Health Network, Toronto, for their help in the optical mapping analysis. We thank Y. Liu from Osaka University, Japan, for her help in quantifying the platelet coverage on the AngioChip in the blood perfusion study. We thank J. W. Miklas and Y. Xiao for their helpful discussion regarding human cardiomyocyte culture and cell seeding. We thank A. Sofla for his help with the POMaC synthesis. We thank A. Keating and I. Rashedi for providing hMSCs and Y. Zhao for her help in culturing and expanding hMSCs. We thank J. Yang for suggestions regarding POMaC synthesis. This work was made possible by the National Sciences and Engineering Research Council of Canada (NSERC) Steacie Fellowship to M.R. This work was also financially supported by the Canadian Institutes of Health Research (CIHR) Operating Grants (MOP-126027 and MOP-137107), the Heart and Stroke Foundation GIA T6946, NSERC–CIHR Collaborative Health Research Grant (CHRPJ 385981-10), NSERC Discovery Grant (RGPIN 326982-10), NSERC Discovery Accelerator Supplement (RGPAS 396125-10) and National Institutes of Health Grant 2R01 HL076485.

## Author contributions

B.Z. developed the AngioChip concept, designed and performed experiments, analysed data and prepared the manuscript. M.M. contributed to mechanical testing, polymer characterization, sprouting assay, blood perfusion experiments, and vascular anastomosis surgery. M.D.C. performed the primary rat hepatocyte isolation and urea assay. S.O. differentiated hESC-derived hepatocytes. A.K. performed polymer mechanical testing. A.P. differentiated hESC-derived cardiomyocytes and contributed to the whole blood perfusion experiment and optical mapping. L.A.W. performed extraction of human whole blood. S.M. and K.N. performed optical mapping measurements and analysis. J.K. performed mass spectrometry analysis. L.R. contributed to the direct vascular anastomosis surgery; A.M. performed the direct vascular anastomosis surgery; S.S.N. contributed to the direct vascular anastomosis surgery and writing of the manuscript. A.R.W. contributed to the writing of the manuscript. G.K. contributed to the writing of the manuscript. M.V.S. contributed to writing of the manuscript. M.R. developed the AngioChip concept, supervised the work and wrote the manuscript.

## Additional information

Supplementary information is available in the online version of the paper. Reprints and permissions information is available online at www.nature.com/reprints. Correspondence and requests for materials should be addressed to M.R.

## Competing financial interests

The authors declare competing financial interests: details accompany the paper at http://www.nature.com/naturematerials. M.R. and B.Z. are amongst co-founders of TARA Biosystems and they hold equity in this company.

## Methods

**POMaC synthesis.** To prepare poly(octamethylene maleate (anhydride) citrate) (POMaC) prepolymer, 1,8-octanediol, citric acid and maleic anhydride were mixed at a 5:1:4 molar ratio and melted at 160 °C under nitrogen purge. The temperature was dropped to 140 °C and the mixture was stirred for 2–3 h. The resultant prepolymer solution was then dissolved in 1,6-dioxane and purified through drop-wise precipitation in deionized distilled water produced from a Direct-Q 5 Water Purification System (Millipore). Precipitated polymer was collected and lyophilized for 2 days. Before photo-crosslinking, POMaC prepolymer was mixed with 5% (w/w) ultraviolet initiator (Irgacure 2959, Sigma) by melting briefly at around 90 °C. To make nanoporous scaffolds, the POMaC polymer was also mixed with a porogen, poly(ethylene glycol) dimethyl ether (PEGDM, $M_n \sim 500$, Sigma), at 60% (w/w) (Supplementary Fig. 1). Pore-free scaffolds were made without adding PEGDM.

**AngioChip fabrication.** Each layer of the AngioChip scaffold was first generated in AutoCAD and translated to individual SU-8 masters using standard soft lithography techniques as described previously[57] (Supplementary Fig. 3 (step 1)). Micro-hole design was directly incorporated in the AutoCAD drawing for AngioChip scaffolds with micro-holes. Experiments performed using AngioChips with micro-holes were explicitly specified. In AutoCAD, the outer dimensions of the AngioChip were set to 5 mm length, 3.1 mm width and one layer thickness of 150–300 μm. Silicone elastomer (poly(dimethylsiloxane), PDMS, 1:15 crosslinker ratio) was moulded against the SU-8 masters and cured at room temperature for 2–3 days (Supplementary Fig. 3 (step 2)). Patterned PDMS moulds for the base layer and upper layers of the 3D scaffold were capped to glass slides and flat PDMS sheets, respectively (Supplementary Fig. 3 (step 3)). The POMaC solution was then injected into the patterned network through an inlet and outlet and left overnight at room temperature. Injection was achieved either by a syringe pump applying a gentle pressure to push the POMaC solution through the mould without delaminating the mould or by a drop of the polymer solution applied on top of the inlet holes with a gentle positive pressure. Overnight, the POMaC solution filled the entire PDMS moulding including the vertical column extending out from the main mesh network. The gentle positive pressure at the inlet pushed out any trapped air inside the mould because the PDMS was porous and allowed air to escape (Supplementary Fig. 3 (step 4)). Next, injected POMaC solution was crosslinked under ultraviolet light at an intensity of 10 mJ $cm^{-2}$ s for 4 min, for the polymer mixed with the porogen, 60%(w/w) PEGDM/POMaC solution, or 10 min if no PEGDM was added. Afterwards, the PDMS moulds were uncapped and the patterned polymer structures were exposed (Supplementary Fig. 3 (step 5)). The patterned POMaC sheets for the first layer were attached onto the glass slides and the patterned POMaC sheets for the following layers were attached onto the PDMS moulds. The exposed POMaC sheets on the PDMS moulds were then aligned to and pressed against the patterned POMaC sheets on the glass slides with a customized ultraviolet mask aligner (Q2001, Quintel; Supplementary Fig. 3 (step 5)). To bond the layers together, the samples were then exposed to ultraviolet at an intensity of 10 mJ $cm^{-2}$ s for 4 min or 10 min if no PEGDM was added. After the ultraviolet light exposure, the PDMS moulds were released, leaving the two patterned POMaC sheets bonded together and attached to the glass slides (Supplementary Fig. 3 (step 5)). This process was repeated to bond additional patterned POMaC sheets to the established base structure (Supplementary Fig. 3 (step 6)). Finally, fabricated scaffolds were immersed in phosphate-buffered saline (PBS) to release them from the glass slides and incubated overnight at room temperature to leach out the PEGDM porogen. Multiple scaffolds were patterned in parallel on a single glass slide in a single process (Fig. 1a). Additional tips for AngioChip scaffold fabrication are described in Supplementary Methods. AngioChip scaffold structure, degradation properties, burst pressure, mechanical properties and permeability were characterized as described in the Supplementary Methods. Material biocompatibility *in vivo* was assessed as described in Supplementary Methods.

**Bioreactor design.** The bioreactor was composed of four components: a cap, a polycarbonate body, a PDMS base, and a polycarbonate base (Fig. 1c and Supplementary Fig. 6). The bioreactor was designed to accommodate three scaffolds in separate chambers at a time. The polycarbonate body (2.5 cm thick) included 9 wells positioned in three rows: the top row encompassed the inlet wells; the middle row encompassed the main wells, where the AngioChip scaffolds were positioned; and the bottom row encompassed the outlet wells. The PDMS slab (1 mm thick) included three trenches (700 μm deep) where the AngioChip scaffolds were situated. At the bottom of the trenches, micro-posts (200 μm tall) were patterned to lift the AngioChip scaffolds up from the base so that cells/gel can penetrate underneath the scaffolds and encapsulate the entire scaffolds. The trench also included an open inlet and outlet channel where the inlet and outlet of the AngioChip scaffolds could precisely fit. After the AngioChip scaffolds were positioned, the PDMS base was then sandwiched between the polycarbonate base and the polycarbonate body so that the open inlet and outlet channels on the PDMS base were capped with the inlet and outlet of the AngioChip fitted within. The three components were secured with stainless-steel screws.

When assembling the AngioChip scaffold into the bioreactor, it is crucial to not apply excessive pressure onto the scaffold inlet and outlet by screwing the bioreactor too tight. Excessive pressure applied could constrict the inlet and outlet channel and reduce the flow rate. To prevent leakage of fluid around the inlet and outlet of the scaffold, a drop (around 10 μl) of 1% (w/v) agarose solution sterilized and heated to 80 °C can be applied around the connection of the inlet and outlet to seal any gaps (Fig. 1c (step 1)).

After assembling the scaffold onto the bioreactor, the bioreactor was filled with culture media and incubated at 37 °C to prime the scaffold overnight, before cell seeding. As the assembly was done at room temperature, when the bioreactor was placed in the incubator at 37 °C, the increase in temperature could lead to the expansion and elimination of any bubbles trapped within the scaffold network. Ethanol should not be used to prime the scaffold at this stage because ethanol significantly swells the scaffold and results in failure in the inlet and outlet connection (Fig. 1c (step 1)).

Solution and/or cell suspensions were perfused from the inlet wells through the built-in networks of the AngioChip scaffolds to the outlet wells driven by a pressure-head difference between the inlet and outlet wells (Supplementary Fig. 7). The bioreactor was disassembled in sterile conditions to remove the AngioChip tissues for implantation or analysis. When applying parenchymal cells in hydrogel around the scaffold, 10 μl of the gel/cell suspension was first applied to the scaffold, allowing the cells to fall through the lattice matrix of the scaffold to fill the space under the scaffold as well as the lattice matrix. Then, after 10 min of incubation at 37 °C, an additional 5 μl of the gel/cell suspension was applied on top of the scaffold to fully encase the scaffold in gel/cell suspension. This sequential seeding method helped ensure more even seeding. If all the gel/cell suspension was applied at once, the scaffold would tend to float to the surface of the suspension and result in less cell/gel on the upper surface of the scaffold (Fig. 1c (step 3)). To examine the fluid flow through the AngioChip scaffold in the bioreactor, AngioChip scaffolds with 10 μm micro-holes and without endothelial cell coating were perfused by adding 4 ml of PBS in the inlet wells and 1 ml of PBS in the main wells. After 24 h incubation at 37 °C, the PBS was collected from the inlet, main and outlet wells and weighed to determine fluid distribution in different compartments.

**Cell maintenance and differentiation.** Human umbilical vein endothelial cells (HUVECs) were purchased from Lonza and cultured with endothelial growth medium (EGM2, Lonza). Lewis rat vein endothelial cells were purchased from CellBiologics and cultured with Complete Rat Endothelial Cell Medium (CellBiologics). Human mesenchymal stem cells (hMSCs) were gifts from A. Keating's laboratory at University Health Network, Toronto, Canada. hMSCs were isolated from a healthy person under 40 years of age. hMSCs were expanded and cultured in Dulbecco's modified Eagle medium (Gibco) with 10% (v/v) fetal bovine serum (Gibco), 1% (v/v) HEPES (100 units $ml^{-1}$, Gibco) and 1% (v/v) penicillin–streptomycin (100 mg $ml^{-1}$, Gibco). Undifferentiated H9 (WA09) human embryonic stem cells (hESCs), purchased from The Wicell Research Institute, were maintained, differentiated into hepatocytes and cultured as previously described[46,58]. To inhibit notch signalling, gamma-secretase inhibitor (GSI) L-685,485 (10 μM, Tocris) was included in the medium throughout the culture period on AngioChip. Primary rat hepatocytes were isolated using a modified two-step isolation procedure from 8-week-old male Sprague Dawley rats[59], according to a protocol approved by the University Toronto Animal Care Committee. Neonatal rat cardiomyocytes and fibroblasts were isolated by digesting neonatal rat hearts as described previously, according to a protocol approved by the University of Toronto Animal Care Committee[57]. HES-3 NKX2-5 GFP-positive cells, provided by G. Keller, were maintained, differentiated to human cardiomyocytes, and cultured using previously described techniques[60,61]. Cells have not been tested in house for mycoplasma contamination. All cell lines were individually stored and logged into the inventory system.

**Endothelialization and tissue assembly.** To enhance cell attachment onto the AngioChip scaffolds as well as within the internal network, the scaffolds were coated with 0.2% (w/v) gelatin (from porcine skin, Type A, Sigma) in PBS for 2 h before assembly. To prevent cell attachment onto the PDMS base, it was coated with 5% (w/v) Pluronic F-127 (Sigma) in PBS for 2 h before assembly. After the AngioChip scaffolds were placed in the bioreactor, endothelial cells were first seeded into the built-in network of scaffolds by perfusing 10–20 μl of concentrated endothelial cell suspension (25 million cells $ml^{-1}$) in endothelial cell media into the network for 1 min. The flow was then stopped to allow the cells to attach under static conditions for 2 h. Unattached cells were then flushed by adding 1 ml of endothelial cell media to the inlet wells, thus initiating perfusion through AngioChip scaffolds under a flow rate less than 0.7 μl $min^{-1}$ (0.62 dyne $cm^{-2}$, Re, 0.01) to apply minimal stress to the cells while feeding the cells with sufficient media. After 2 h incubation, 3 ml of EC medium was then added to increase the flow rate to near a one-day average perfusion rate of 0.7 μl $min^{-1}$. Within the

network, the endothelial cells were allowed to proliferate and form a confluent network overnight (the bioreactor can be temporarily tilted at 45° angle to increase perfusion rate and accelerate EC proliferation overnight). Before the seeding of parenchymal cells, all EC media were removed from the bioreactor. On day 1, to create an AngioChip hepatic tissue, primary adult rat hepatocytes or hESC-derived hepatocytes mixed with 20% hMSCs were seeded at 100–200 million cells $ml^{-1}$ with 15 µl Matrigel (BD Biosciences) onto the AngioChip scaffolds. To create a rat AngioChip cardiac tissue, cardiomyocytes isolated from neonatal rats were seeded with 15 µl (single-layer network) collagen/Matrigel mixture at 100–200 million cells $ml^{-1}$ onto each AngioChip scaffold. The composition of the collagen/Matrigel mixture was as follows: 2.5 mg $ml^{-1}$ of rat tail collagen type I (BD Biosciences) neutralized by 1 N NaOH and 10× M199 medium as described by the manufacturer, supplemented with 4.5 µg $ml^{-1}$ glucose, 1% HEPES, 10% (v/v) Matrigel (BD Biosciences), and 2 µg $ml^{-1}$ $NaHCO_3$. To create a human AngioChip cardiac tissue, hESC-derived cardiomyocytes mixed with or without 10% hMSCs were seeded with 15 µl (single-layer network) Matrigel (BD Biosciences) at 100–200 million cells $ml^{-1}$ onto each AngioChip scaffold. After 30 min gelation at 37 °C, 1 ml of hepatocyte medium or cardiomyocyte medium was added to the middle well. After the seeding of parenchymal cells, an additional 4 ml of endothelial cell medium was also added to the inlet wells, increasing medium perfusion rate back to a one-day average perfusion rate of 0.7 µl $min^{-1}$ (0.62 dyne $cm^{-2}$, Re, 0.01). As a control, hepatocyte collagen sandwich culture was used by first plating hESC-derived hepatocytes with 20% hMSCs on 48-well plates (0.14 million cells per well). Attached cells were then encapsulated with collagen (500 µl per well). As a control for cardiac cell culture, cardiac Biowires were formed by seeding hESC-derived cardiomyocytes with 10% hMSCs around a surgical suture according to a previously published protocol[5]. Cardiac monolayer culture was formed by seeding hESC-derived cardiomyocytes with 10% hMSCs on 96-well plates (0.02 million cells per well).

Thick cardiac tissues were assembled by centrifugation-facilitated cell seeding of the thick AngioChip scaffolds with 20 µm micro-holes. The built-in network of the AngioChip scaffold was first endothelialized and cultured for one day. Around 30–40 million cells made up of 20% endothelial cells (HUVECs), 20% hMSCs, and 80% hESC-derived cardiomyocytes were mixed with 40 µl of fibrinogen (33 mg $ml^{-1}$). A total of 40 µl parenchymal cell solution was pipetted onto each thick scaffold at once followed by centrifugation at 87*g* for 3 min. Alternatively, three batches of 14 µl cell solution were sequentially pipetted followed by centrifugation after each batch at 28–87*g* for 1 min (the centrifuge should be well balanced to ensure a smooth spinning-speed acceleration). Finally, 5 µl of thrombin (25 U $ml^{-1}$) was added to the top of the tissue to induce gelation. Seeding with Matrigel was performed in a similar fashion only with the temperature control set at 4 °C. An extended bioreactor column was added to the bioreactor to increase the height of the bioreactor chambers to generate a higher-pressure head to increase perfusion for the thick tissue. Fifty millilitres of endothelial cell medium was added to the inlet chamber and 15 ml of cardiomyocyte medium was added to the main chamber of the AngioChip bioreactor. Both media were supplemented with 10 µg $ml^{-1}$ aprotinin.

For the tissue stacking approach, three endothelialized single-layer AngioChip cardiac tissues were seeded with human cells and cultured as described above for three days. They were then removed from their individual bioreactor wells and then stacked onto each other in a new bioreactor with a 1.5-mm-deep main tissue well. The three tissues were held in place during cultivation with U-shaped stainless-steel micro-pins.

**Tissue characterization.** Endothelial sprouting from AngioChip, whole blood perfusion, monocyte and macrophage adhesion and migration on the AngioChip vasculature were performed as described in detail in the Supplementary Methods. Histology, immunostaining and quantification of cell density in AngioChip hepatic and cardiac tissues were assessed as described in the Supplementary Methods. Urea assays on hepatic tissue and liver drug testing were performed as described in the Supplementary Methods. Functional characterization of engineered cardiac tissue, lactate dehydrogenase assays on cardiac tissue and cardiac drug testing were performed as described in the Supplementary Methods.

**Rat femoral vessel surgery.** All procedures below were performed at the Department of Comparative Medicine Animal Facility, University of Toronto, under a protocol approved by the Committee on Animal Care. AngioChip scaffolds alone, those cultured with Lewis neonatal rat cardiomyocytes, or endothelialized AngioChip scaffold cultured with Lewis neonatal rat cardiomyocytes on day 7 were used for the implantation experiments. Lewis rat vein endothelial cells (CellBiologics) isolated from inferior vena cava tissue of 6–8-week-old Lewis rats were used to endothelialize the AngioChip scaffolds for implantation. To demonstrate the ability of AngioChip to be implanted in two different ways with direct anastomosis *in vivo*, we used two different configurations: artery bypass configuration and artery-to-vein configuration. To improve the mechanical stability of the anastomosis site, the inlet and outlet segment of the AngioChip scaffold were made without the use of porogen. During the surgery, adult male Lewis rats (150–250*g*) from Charles River were first anaesthetized with 1–3% isoflurane at flow rate of 1 l $min^{-1}$. Analgesic was administered (5 mg $kg^{-1}$ ketoprofen, SQ) and both hindlimbs were prepared for surgery. For the surgical procedure, a dissection microscope was used to obtain an enlarged view of the hindlimb region. Skin was shaved and incisions were made on the left leg, approximately 2 cm long starting from the knee to the medial thigh. Then, subcutaneous fat tissue and the underlying neurovascular bundle were revealed. The femoral artery and vein were dissected and separated from the nerve. For the artery bypass configuration, a segment of the femoral artery (approximately 1.5 cm in length) was fully exposed and ligated for the insertion of the AngioChip cardiac tissue. The two ends of the artery were clamped with a microsurgical approximating clamp to temporarily stop blood flow during the surgery. One 25 gauge cuff (polyimide tube) was inserted into each end of the artery and secured with 7-0 sutures. Biodegradable surgical cuffs can also be used in future applications[62]. The inlet and outlet of the AngioChip cardiac tissue were then inserted into the cuffs and sealed with tissue glue (Cyanoacrylate). Clamps were then removed and blood perfusion was established. For the artery-to-vein configuration, a segment (approximately 5 mm in length) of the femoral artery and femoral vein was fully exposed and ligated for the insertion of the AngioChip cardiac tissue. The ends of the artery and vein were clamped with a microsurgical approximating clamp to temporarily stop blood flow during the surgery. One 25 gauge cuff (polyimide tube) was inserted into each top end of the artery and vein and secured with 7-0 sutures. The bottom ends of the artery and vein were sealed with 7-0 sutures. The inlet and outlet of the AngioChip cardiac tissue were then inserted into the cuffs and sealed with tissue glue (Cyanoacrylate). Clamps were then removed and blood perfusion was re-established. Last, another cardiac tissue patch was implanted to the right leg subcutaneously in a similar manner but without anastomosis to serve as a control. For post-operative pain management, rats received ketoprofen (5 mg $kg^{-1}$, subcutaneous injection daily) for 2 days. At the 1-week time point the animals were humanely euthanized and the tissue implants were isolated for histology sectioning.

**Statistical analysis.** Significant differences between experimental groups were determined using independent two-tailed Students' *t*-test unless specified otherwise. In Fig. 2f, one-way analysis of variance (ANOVA) was used with a normality test (Shapiro–Wilk) and pairwise multiple-comparison procedures (Holm–Sidak method). In Fig. 4g, Kruskal–Wallis one-way ANOVA on ranks was used and followed by pairwise multiple comparison procedures (Student–Newman–Keuls method). In Fig. 5z, two-way repeated measures ANOVA was used with a normality test (Shapiro–Wilk) and followed by pairwise multiple comparison procedures (Holm–Sidak method). $p < 0.05$ was considered significant for all tests.

## References


57. Zhang, B., Green, J. V., Murthy, S. K. & Radisic, M. Label-free enrichment of functional cardiomyocytes using microfluidic deterministic lateral flow displacement. *PLoS ONE* **7,** e37619 (2012).
58. Ogawa, M. *et al*. Directed differentiation of cholangiocytes from human pluripotent stem cells. *Nature Biotech.* **33,** 853–861 (2015).
59. Berry, M. & Friend, D. High-yield preparation of isolated rat liver parenchymal cells: a biochemical and fine structural study. *J. Cell Biol.* **43,** 506–520 (1969).
60. Kennedy, M., D'Souza, S. L., Lynch-Kattman, M., Schwantz, S. & Keller, G. Development of the hemangioblast defines the onset of hematopoiesis in human ES cell differentiation cultures. *Blood* **109,** 2679–2687 (2007).
61. Lian, X. *et al*. Directed cardiomyocyte differentiation from human pluripotent stem cells by modulating Wnt/β-catenin signaling under fully defined conditions. *Nature Protocols* **8,** 162–175 (2013).
62. Zeebregts, C., Heijmen, R., Van Den Dungen, J. & Van Schilfgaarde, R. Non-methods of vascular anastomosis. *Br. J. Surg.* **90,** 261–271 (2003).